COBEM 2023 27TH INTERNATIONAL CONGRESS OF MECHANICAL ENGENEERING

ABCM Brazilian Society of Mechanical Sciences and Engineering
27th ABCM International Congress of Mechanical Engineering
December 04-08, 2023, Florianópolis-SC, Brazil

COBEM-2023-2060
EXPERIMENTAL METHODS FOR IDENTIFYING PHYSICAL PARAMETERS OF FOUR-WHEELED AUTONOMOUS VEHICLES

João Victor A. P. Bezerra
Felipe W. Varga
Ely C. de Paiva
Niederauer Mastelari
Faculty of Mechanical Engineering, University of Campinas (FEM/UNICAMP), Campinas, SP, Brazil
j230813@dac.unicamp.br, f234341@dac.unicamp.br, elypaiva@unicamp.br, niede@unicamp.br
Rafael A. Cordeiro
Department of Electrical Engineering, Federal University of Espírito Santo, Vitória, ES, Brazil
rafael.cordeiro@ufes.br
Mauro F. Koyama
Center for Information Technology Renato Archer, Campinas, SP, Brazil
mauro.koyama@cti.gov.br

Abstract. *Four-Wheeled Autonomous Vehicle have emerged as an innovative technology with significant potential to revolutionize the transportation industry. In the past decade, the research efforts in this field aim to develop strategies ranging from the development of Advanced Driver Assistance Systems (ADAS) up to the creation of fully autonomous navigation strategies. In this context, mathematical models of the four-wheeled robots are an essential part of developing autonomous navigation techniques. Whether using complete or simplified mathematical models of the vehicle, the control synthesis requires accurate model parameters. The physical parameters of the platform must be provided in an accurate way for these models. In this paper, we present experimental methods to obtain some of the main physical parameters that determine the dynamic model of four-wheeled vehicles, including its mass, center of gravity, and principal moments of inertia. The uncertainties of this measurements are presented with the aim of providing an estimate of the reliability and precision of the results obtained. We also present a cornering stiffness estimation method based on the vehicle lateral dynamics and an experimental dataset. Experimental results obtained from a four-wheeled 1:5 scaled electrical vehicle, with real electronic differential distribution are presented.*

Keywords: *Dynamical models, Vehicle dynamics, cornering stiffness, Experimental methods, Parameters determination*

1. INTRODUCTION

In the recent years, there has been significant research attention dedicated to autonomous vehicles driving technology, both in academy as well as in industry. Many companies and research laboratories have been looking for improvements in performance, safety and comfort of self-driving cars (Lutin, 2018). The use of a scaled-robotic vehicles is a way to demonstrate and facilitate the investigations in autonomous vehicle control and sensing systems. Researchers often resort to using car-like robots that shorten the path of building, testing, validating, and scaling algorithms for large cars (Goldfain *et al.*, 2019), (Polley and Alleyne, 2004).

This is the case in our work, that is part of the VERDE project (Robotic Electric Vehicle with Electronic Differential) (Nogueira *et al.*, 2019). The VERDE prototype is a four-wheeled 1:5-scaled vehicle, which has an electronic differential distribution for an optimized torque/speed distribution, aiming at autonomous driving applications in aggressive environments, like in agricultural applications, under slippery and highly uneven terrains (Lemos *et al.*, 2017),(Bonacini *et al.*, 2023), (Ribeiro *et al.*, 2022). The VERDE, shown in Figure 1, vehicle is a fully instrumented platform with inertial navigation system INS/GPS, on-board computer, CAN bus, long-distance laser scan (30 meters), camera, and sensors for measuring wheel speed and steering.

Most developments in autonomous navigation techniques require an accurate knowledge of the vehicle model (Cordeiro, 2013). Providing accurate physical parameters is crucial for vehicle models to ensure reliable, high-performance, and safe vehicular systems. Numerous studies have been conducted in searching of techniques to accurately estimating vehicle parameters in order to enhance their reliability and performance (Cordeiro *et al.*, 2014), (Ribeiro *et al.*, 2021).

This work presents experimental methods to identify fundamental vehicle parameters such as vehicle mass, center of gravity (CG), and principal moments of inertia in the x, y, and z directions, using standard weighing scales and pendulums. The measurements of these parameters and their respective uncertainties were obtained by applying the uncertainty analysis presented by Taylor (Taylor, 1997), to evaluate the quality of measurements and methods used. We also propose

Figure 1: VERDE robotic platform.

a cornering stiffness estimation method based on the lateral dynamics of the vehicle and an experimental dataset, taking into account the different characteristics of the front and rear tires.

This paper is organized as follows: section 2 presents the methods and techniques employed in this work. Section 3 shows the experimental setups and results and section 4 presents the final conclusions.

2. APPROACH FOR PARAMETER IDENTIFICATION: METHODS AND TECHNIQUES

In this section, we present the methodology employed for obtaining the main parameters required for the dynamic modeling of a terrestrial robotic vehicle. We describe the techniques and methods for identifying these parameters, which are essential for analyzing the dynamics of vehicles.

2.1 Mass

The main parameter for modeling vehicle dynamics is its total mass. The mass of the vehicle can be obtained directly through the use of scales. To carry out the measurements, we use four scales positioned under each wheel and they are place over a flat surface. The static equilibrium analysis of the free-body diagram shown in Figure 2 leads to:

$$\frac{F_z^{FL}}{g} + \frac{F_z^{FR}}{g} + \frac{F_z^{RL}}{g} + \frac{F_z^{RR}}{g} = m \tag{1}$$

The indices FL, FR, RL, and RR correspond to the front-left, front-right, rear-left, and rear-right corners, respectively, and g is the gravitational acceleration.

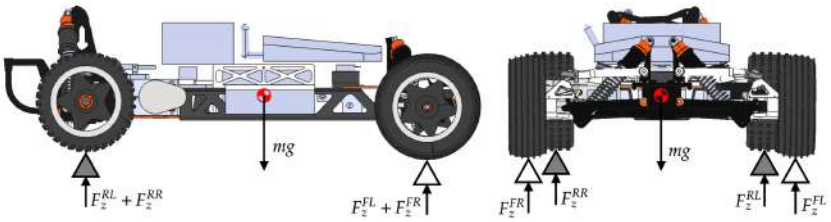

Figure 2: Free body diagram of the vehicle.

2.2 Center of gravity

The position of the Center of Gravity (CG) is required for modeling the vehicle dynamics. Figure 3 shows the parameters that provide the position of the vehicle Center of Gravity.

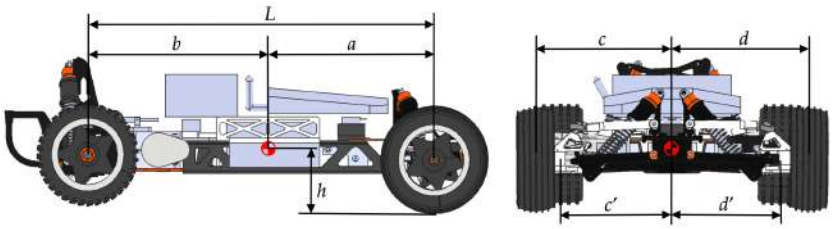

Figure 3: Location of Center of Gravity.

The dimensions a, b, c, d, c', and d' are defined from fixed points of the vehicle body, and h is defined with respect to the lower end of the vehicle.

To determine these parameters, it is necessary to measure the normal forces at each of the vehicle extremities in two situations: with the vehicle on a horizontal plane, to ensure an uniform load distribution, and with the vehicle on an inclined plane (Jazar, 2008). In the case of the horizontal plane, the static equilibrium analysis in the x-axis rotation results in:

$$(F_z^{FL} + F_z^{FR})a = (F_z^{RL} + F_z^{RR})b \tag{2}$$

This leads us to a scenario with one equation and two unknowns. The second equation can be derived by considering that the parameter *(a+b)* represents the distance between the front and rear wheel axles of the vehicle, which is a known value.

Similarly, *c* and *d* dimensions can be determined by the normal forces measurements and the static equilibrium analysis in the y-axis rotation. Since the rear track width is smaller than the front track width, the torques generated by the rear wheels are functions of *c'* and *d'*. Therefore, the static analysis provides:

$$F_z^{FR}c + F_z^{RR}c' = F_z^{RL}d' + F_z^{FL}d \tag{3}$$

The remaining equations to solve for c, can be derived by the sum $(c + d)$ and $(c' + d')$, which are equal to the front and rear track distances, respectively, and the linear relation between the distances given by $c - c' = d - d'$. To obtain the height h of the CG, we must measure the support forces of the vehicle on an inclined plane, at a known angle θ with respect to the ground plane. By balancing the sum of torques in the y-axis direction on point O (center of front wheel), see Figure 4, the height h can be obtained from Eq. (4).

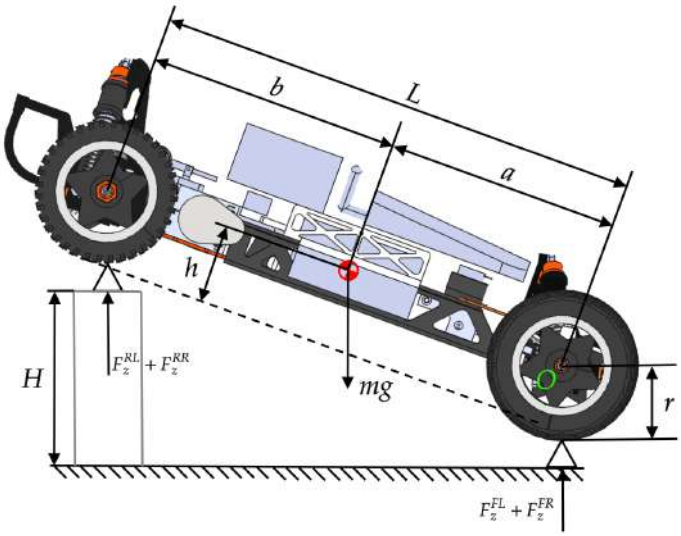

Figure 4: Forces diagram of inclined vehicle experiment.

$$h = \frac{-(F_z^{RL} + F_z^{RR})L\cos\theta + mg(a\cos\theta + r\sin\theta)}{mg\sin\theta} \tag{4}$$

According to (Uys *et al.*, 2006) the accuracy of the value of *h* increases as the slope increases and then obtains results that suggest that the angle θ must be above $10°$.

2.3 Main moments of inertia

The moments of inertia play a crucial role in vehicle dynamics as they are directly linked to angular motions. The principal moments of inertia capture the mass distribution around the principal axes, with the origin located at the center of gravity. The moment of inertia provides valuable insights into the vehicular dynamics.

In (Schedlinski and Link, 2001) several methods for measuring moments of inertia are described, classifying them as: a) methods without movement limits, b) methods with low angular movement, and c) methods with very low angular movement.

A widely-used method for measuring moments of inertia involves pendulums (Dunmore, 1961), (Schedlinski and Link, 2001). This approach, although simple and accurate, requires performing six separate tests to obtain the parameters of the inertia tensor.

By assuming a symmetric mass distribution of the vehicle across the *x, y*, and *z* axes, the coordinate system aligns with the principal axes of rotation. Consequently, the cross-parameters can be disregarded, resulting in a reduction to three required tests (Cordeiro *et al.*, 2014).

The first method applied is the single pendulum, commonly employed to determine the moments of inertia around the x and y axes. This method allows for experimentation with the vehicle in a horizontal position, ensuring enhanced safety during the procedure. The measurement using a simple pendulum relies on the direct application of the Newton-Euler motion equation. As shown in Figure 5, the body is suspended by strings, and a controlled rotation around the axis (in this case, *x* or *y*) is induced. Consequently, for small angles:

$$I'_x\ddot{\phi} + mgL_{CG}\phi = 0 \tag{5}$$

$$I'_y\ddot{\theta} + mgL_{CG}\theta = 0 \tag{6}$$

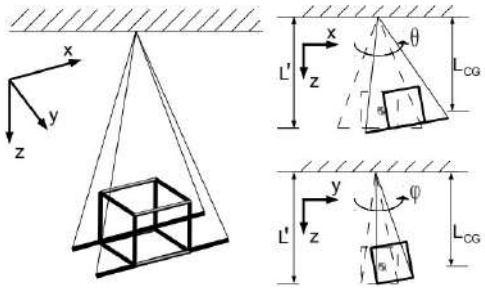

Figure 5: Simple gravitational pendulum.

Here, L' represents the length of the equivalent pendulum, and L_{CG} denotes the distance between the pendulum rotation axis and the CG of the vehicle, specifically given by $L_{CG} = L' - h$. It is important to note that this analysis assumes an ideal pendulum, devoid of any friction or air resistance, thus:

$$\phi = \sin(2\pi f_\phi t) \tag{7}$$

$$\theta = \sin(2\pi f_\theta t) \tag{8}$$

Let f_ϕ and f_θ denote the oscillation frequencies relative to the x and y axes, respectively. By performing a double time-derivatice in Eq. (7) and Eq. (8) with respect to time and replacing them into Eq. (5) and Eq. (6), respectively, we derive the following expressions:

$$I'_x = \frac{mgL_{CG}}{(2\pi f_\phi)^2} \tag{9}$$

$$I'_y = \frac{mgL_{CG}}{(2\pi f_\theta)^2} \tag{10}$$

Nevertheless, the inertia values calculated by Eq. (9) and Eq. (10) are determined with the axes passing through the point of attachment of the pendulum strings. To obtain the moment of inertia about the CG, it is imperative to employ the Huygens-Steiner theorem (Gobbi *et al.*, 2011), commonly referred to as the Parallel Axis Theorem. Therefore, the moments of inertia with respect to the x and y axes are determined by the following equations:

$$I_x = \frac{mgL_{CG}}{(2\pi f_\phi)^2} - mL_{CG}^2 \tag{11}$$

$$I_y = \frac{mgL_{CG}}{(2\pi f_\theta)^2} - mL_{CG}^2 \tag{12}$$

For the determination of I_z, the use of torsional pendulums is a simpler and safer alternative compared to the simple pendulum method (Dunmore, 1961), (Schedlinski and Link, 2001). In the implementation of the torsional pendulum, two or more wires are employed to support the vehicle, and a torsional force is applied to the pendulum. As a result of the rotation, the vehicle elevates, converting the kinetic energy of motion into potential energy (Nestorides, 1958). Figure 6 illustrates a representation of the torsional pendulum.

Considering the depicted configuration in Figure 6, where the cables are arranged orthogonally to the vehicle frame, an analysis of the potential energy and geometry allows for the determination of the inertia along the z-axis. By employing this approach, the equation for the I_z can be expressed by Eq. (13).

$$I_z = \frac{mgB^2}{L'(2\pi f_\psi)^2} \tag{13}$$

Where B is the radius achieved by the torsional pendulum and f_ψ is the frequency of oscillation around the z-axis.

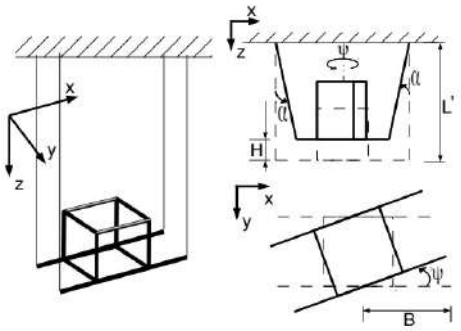

Figure 6: Multifilar torsional pendulum.

2.4 Tire cornering stiffness

Cornering stiffness lays a crucial role in the lateral vehicle dynamics model as it directly influences the vehicle behavior and stability. The accurate value of cornering stiffness in the model is vital for predicting and analyzing the vehicle lateral response.

In order to estimate the cornering stiffness we employed a vehicle bicycle model as the basis, due to it provides a description of the lateral and yaw dynamics of the vehicle (Snider, 2009). A representation of the bicycle model is presented in Figure 7.

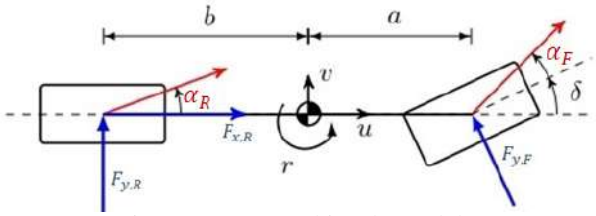

Figure 7: 2D-yaw bicycle model.

Considering the forces in the free-body diagram, and applying the Newton second law, the mathematical model is achieved (Rajamani, 2011).

$$ma_y = F_{y,R} + F_{y,F}\cos\delta \tag{14}$$

Where a_y is the lateral acceleration, *u* is the longitudinal speed, *r* is the angular velocity around the z-axis, and δ is the front-wheel steering angle. For the front wheel the longitudinal slip will be considered negligible, *i.e.*, $F_{x,F} \approx 0$.

The lateral force is modeled as linearly dependent on the slip angle in the corresponding wheel (considering low speeds and good grip):

$$F_{y,W} = -2C_{\alpha,W}\alpha^W \tag{15}$$

Where the sub-index W can be R (rear wheel) or F (front wheel), and α^W is the angle between the wheel velocity and the longitudinal axis of the vehicle, defined as follow:

$$\alpha^F = \arctan\left(\frac{v+ar}{u}\right) - \delta \tag{16}$$

$$\alpha^R = \arctan\left(\frac{v-br}{u}\right) \tag{17}$$

By substituting Eq. (15), Eq. (16), and Eq.(17) into Eq. (14) and linearizing, we obtain (Sierra *et al.*, 2006):

$$ma_y = \left(\frac{v+ar}{u} - \delta\right)C_{\alpha,F} + \left(\frac{v-br}{u}\right)C_{\alpha,R} \tag{18}$$

Where *v* is the lateral velocity of the vehicle. The signals a_y, v, u, and r can be obtained (directly or indirectly) by sensors, thus transforming the problem into a system of one equation and two unknowns. To address this problem

and find a solution, we use a cost function J, which quantifies the discrepancies between the estimated values $\hat{y}$ and the corresponding measured value (y_{real}). The cost function J is defined as the sum of squared errors, given by:

$$J(C_{\alpha,W}) = \frac{1}{2n}\sum_{i=1}^{n}(\hat{y}^{(i)} - y_{real}^{(i)})^2 \tag{19}$$

Where n is the total number of data points acquired. By minimizing this cost function, we aim to optimize the parameters $C_{\alpha,W}$ and find the values that yield the closest match between the estimated and measured values.

To achieve the minimization of the cost function, we employ a gradient descent algorithm (Géron, 2022), which involves iteratively adjusting the parameter values based on the gradient of the cost function J. To update these parameters, we compute the partial derivatives of with respect to $C_{\alpha,F}$ and $C_{\alpha,R}$:

$$\frac{\partial J}{\partial C_{\alpha,F}} = \frac{1}{n}\sum_{i=1}^{n}(\hat{y}^{(i)} - y_{real}^{(i)})C_{\alpha,F} \tag{20}$$

$$\frac{\partial J}{\partial C_{\alpha,R}} = \frac{1}{n}\sum_{i=1}^{n}(\hat{y}^{(i)} - y_{real}^{(i)})C_{\alpha,R} \tag{21}$$

At each iteration, we calculate the gradients, in Eq. (20) and Eq. (21), using the current parameter values. Then, the parameter values are updated as following:

$$C_{\alpha,F}(K+1) = C_{\alpha,F}(K) - \lambda\frac{\partial J}{\partial C_{\alpha,F}(K)} \tag{22}$$

$$C_{\alpha,R}(K+1) = C_{\alpha,R}(K) - \lambda\frac{\partial J}{\partial C_{\alpha,R}(K)} \tag{23}$$

Here, λ is the learning rate, which determines the step size in the parameter update. By iteratively performing these updates, we gradually move towards the optimal values of $C_{\alpha,F}$ and $C_{\alpha,R}$ that minimize the cost function J.

3. PERFORMED TESTS AND EXPERIMENTAL RESULTS

The necessary tests to obtain the parameters described in Section 2 were conducted at the Laboratory for Studies in Outdoor Robotic Vehicles (LEVE) at the University of Campinas (Unicamp).

3.1 Mass and center of gravity

To measure the vehicle mass, four standard scales with a range of 0 to 10kg and accuracy of $\pm$1 g were used. These scales were initially calibrated with an OHAUS precision scale model TP4000D with an accuracy of $\pm$ 0.01 g. These scales were placed under the vehicle tires and positioned on a flat surface. Five direct measurements were conducted to obtain the weight distribution between the scales and the associated uncertainty of each mean value of mass were calculated, with 95% of confidence (Figliola and Beasley, 2021). In the experiments carried out, it is considered that the errors follow a normal distribution.

Using the measured mass values from each scale and applying them in Eq. (1), it was possible to determine the total mass of the vehicle and its uncertainty, by propagating the masses values uncertainties with the partial derivatives of the Eq.(1) (Taylor, 1997). Since the mass measurements were taken on a level surface, resulting in a uniform load distribution, these values can be applied in Eq. (2) to obtain *a* and *b*, representing the distances from the CG to the front and rear of the vehicle, respectively. Figure 8 shows the configuration used to obtain the mass and parameters *a* and *b*. The parameters *c* and *d*, which correspond to the position of the CG along the y-axis, can be determined using the same experimental setup.

To determine the height *h* of the CG, eleven measurements were taken with the rear of the vehicle raised at an angle of $\theta = 17°$. The measured results were used in Eq. (4), and then the average value of the height *h* was calculated. The obtained results for the total mass and CG position of the vehicle and their propagated uncertainties, calculated with the partial derivatives method (Figliola and Beasley, 2021), are presented in Table 1.

The obtained values for the vehicle mass, *a*, *b*, *c* and *d* showed uncertainties values of less than 1%. The value of the height of the center of gravity had a reasonable uncertainty of 5%, although higher than the other distances because of its Eq. (4), that involves more parameters. To determine the CG height of the vehicle we must consider multiple variables, such as the load distribution on each tire, the overall mass of the car, the angle of inclination observed during testing, and the previous calculated CG coordinate *a*. Therefore the result of *h* has more associated errors than the other CG distances.

(a) Experiment on a level surface

(b) Inclined plane experiment

Figure 8: Experiments for obtaining mass and CG

Table 1: Experimental results for the total mass and CG position of the vehicle, with 95% of confidence.

Dimension Description	**Variable**	**Values**
Mass of the car	m	$18.9032 \pm 0.0416\,kg$
Distance from CG to the center of front wheels along the x axis	a	$328.9 \pm 1.2\,mm$
Distance from the center of rear wheels to the CG along the x axis	b	$248.1 \pm 1.3\,mm$
Distance from the middle of right wheels to the CG along the y axis	c	$228.9 \pm 0.8\,mm$
Distance from CG to the middle of left wheels along the y axis	d	$227.1 \pm 1.0\,mm$
Height of the CG	h	$149.3 \pm 7.3\,mm$

3.2 Moments of inertia

As observed in Eq. (11), Eq. (12), and Eq. (13), the moments of inertia around the x, y, and z axes are dependent on their respective oscillation periods. Therefore, four pendulum tests for each moment of inertia were conducted, and an XSENS inertial measurement unit (IMU) was used to generate the oscillation signals, with which the mean period of oscillation were obtained for each experiment. The IMU was positioned near the vehicle CG to accurately measure the angular displacement. The experiments setups for the Moments of inertia are shown in Figure 9. Figure 10 shows the roll, pitch, and yaw angles signals obtained from the pendulum experiments described in Section 2.3.

(a) Single pendulum

(b) Torsional pendulum

Figure 9: Setup of pendulum experiments

Observably, the amplitude of the pendulum oscillations decreases over time. However, the period of oscillation remains constant. Given that the time difference between successive peaks provides us with the oscillation period, the peaks of the oscillations were isolated and marked as red dots in Figure 10. The first ten periods of time were averaged, and the frequencies obtained were then used in Eq. (11), Eq. (12), and Eq. (13). For calculating the associated uncertainties of the time periods, where multiple experiments were done, the Maximum Likelihood Algorithm was used (Figliola and Beasley, 2021). The resulting values and their associated uncertainties are presented in Table 2.

The measurements of I_z showed uncertainty less than 0.5% while the I_x and I_y moments of inertia uncertainties were much greater, this can be explained by the fact that the I_z Equation (13) has less parameters, that is, fewer sources of error than the I_x and I_y equations, Eq. (11) and Eq. (12) respectively, that contains the squared height of the CG in their equations, which by its own, has greater associated uncertainty than the other CG distances.

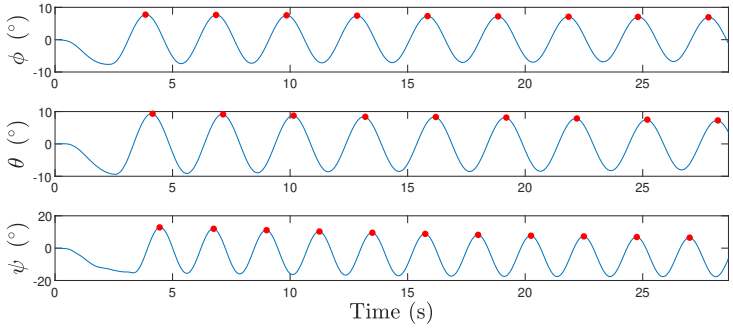

Figure 10: Angular displacements of pendulum experiments.

Table 2: Results for the I_x, I_y and I_z pendulum experiments, with 95% of confidence.

Parameter Description	**Variable**	**Values**
Average time period of the oscillation on the I_x experiment	T_ϕ	$2.9949 \pm 0.0057\, s$
Principal Moment of Inertia along the x axis	I_x	$0.9659 \pm 0.5430\, kg \cdot m^2$
Average time period of the oscillation on the I_y experiment	T_θ	$3.0050 \pm 0.0057\, s$
Principal Moment of Inertia along the y axis	I_y	$1.5913 \pm 0.5409\, kg \cdot m^2$
Average time period of the oscillation on the I_z experiment	T_ψ	$2.2492 \pm 0.0012\, s$
Principal Moment of Inertia along the z axis	I_z	$1.1713 \pm 0.0045\, kg \cdot m^2$

3.3 Cornering stiffness

The cornering stiffness problem, as described in section 2.4, exhibits an under-determinate nature that necessitates persistent excitation for accurate results (Sierra). To achieve this, a varying steering signal was applied to the vehicle using a chirp function as input (Ribeiro et al., 2021). The amplitude of the signal was adjusted within the limits of the vehicle's steering system (up to 0.52 rad), and an example of the input signal is shown in Figure 11.

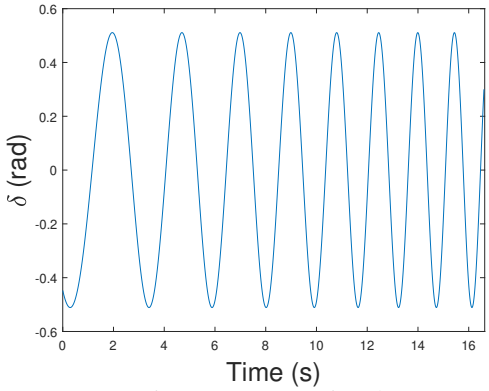

Figure 11: Input signal.

Two classes of sensors are used to collected the data: the E2 incremental optical enconder, responsible for acquiring the values of the longitudinal velocity (u), and the Xsens MTI-G-710 IMU unit, which collects lateral and longitudinal acceleration data and the angular velocity r, wich is directly measured by the IMU's gyroscopes.

The tests were performed on a wet asphalt, the longitudinal speed was set to 1m/s. Lateral velocity was obtained through an Extended Kalman Filter (EKF). Figure 12 shows the signal acquired during the experiment and the values estimated by the EKF. The lateral velocity obtained through the EKF is shown in the Figure 13.

Solving the optimization problem presented in section 2.3 with the data acquired the optimum estimated parameters obtained are $C_{\alpha,F} = 26.5588 N/rad$ and $C_{\alpha,R} = 34.2981 N/rad$. The values obtained through the optimization technique demonstrate a good agreement with the result found in the EKF estimations. For the filter implementation, it was assumed that both rear and front tires had the equal cornering stiffness values, and the obtained equivalent tire stiffness was approximately $30 N/rad$. Finally, the root mean square error (RMSE) was calculated, Eq. (24), resulting in an RMSE

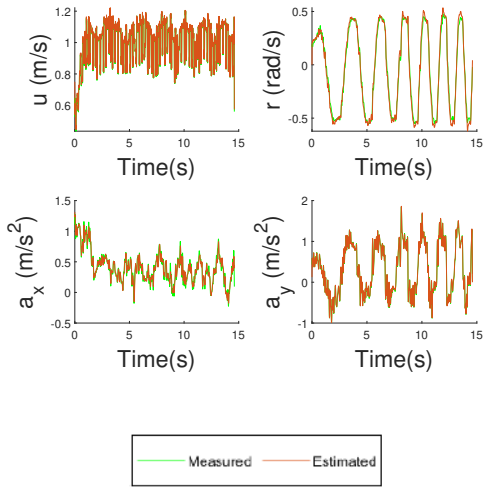

Figure 12: Comparison of measured and EKF-estimated values for a longitudinal velocity of 1m/s.

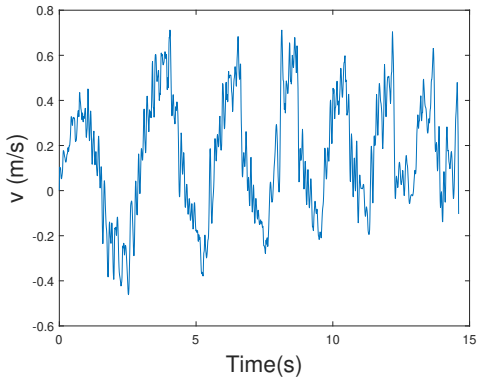

Figure 13: Lateral velocity.

of 1.5929.

$$RMSE = \sqrt{\sum_{i=1}^{n} (\hat{y}^{(i)} - y_{real}^{(i)})^2} \tag{24}$$

4. CONCLUSION

This article outlines methods employed on a scaled electric vehicle in order to identify fundamental mechanical parameters of vehicle dynamics. Experimental setups were proposed, using standard weighing scales and pendulums, to obtain accurate measurements of the vehicle mass, center of gravity (CG), and principal moments of inertia.

A 2D bicycle dynamic model was used to estimated the cornering stiffness of the front and rear vehicle wheels. These methods were able to identify key model parameters that can can greatly impact in controller design and simulator development. The obtained results are consistent with prior knowledge of the system and align with factors such as vehicle structure and geometry.

The results of this article corroborates and extends previous studies of the authors for larger vehicles (Cordeiro *et al.*, 2014), showing that the proposed strategy is scalable for different vehicles. Therefore, the knowledge gained through scaled vehicles can be extrapolated for full-scale vehicles, indicating that design and optimization strategies can be first experimented in scaled vehicle, contributing for enhancing performance and efficiency in developing new commercial vehicle strategies.

5. ACKNOWLEDGEMENTS

This research is part of the INCT InSAC - Autonomous Collaborative Systems - funded by FAPESP proc. 2014/50851-0 and also CNPq procs. 465755/2014-3 and 383165/2022-9.

6. REFERENCES

Bonacini, L., Tronco, M.L., Higuti, V.A.H., Velasquez, A.E.B., Gasparino, M.V., Peres, H.E.N., Oliveira, R.P.d., Medeiros, V.S., Silva, R.P.d. and Becker, M., 2023. "Selection of a navigation strategy according to agricultural scenarios and sensor data integrity". *Agronomy*, Vol. 13, No. 3. ISSN 2073-4395.

Cordeiro, R.A., 2013. *Modelagem e Controle de Trajetória de um Veículo Robótico Terrestre de Exterior*. Master's thesis.

Cordeiro, R.A., Bueno, S.S., Azinheira, J.R., de Paiva, E.C., Pablo, S., Vivan, R., Azevedo, H. and Koyama, M.F., 2014. "Determinação experimental de parâmetros para a modelagem dinâmica de um veículo robótico terrestre". In *XX Congresso Brasileiro de*.

Dunmore, J., 1961. "Handbook on torsional vibrations. british internal combustion engine research association. cambridge university press, london. 1958. 664 pp. illustrated. 110s." *The Aeronautical Journal*, Vol. 65, No. 601, pp. 71–71.

Figliola, R.S. and Beasley, D.E., 2021. *Theory and design for mechanical measurements*. John Wiley & Sons.

Géron, A., 2022. *Hands-on machine learning with Scikit-Learn, Keras, and TensorFlow*. " O'Reilly Media, Inc.".

Gobbi, M., Mastinu, G. and Previati, G., 2011. "A method for measuring the inertia properties of rigid bodies". *Mechanical Systems and Signal Processing*, Vol. 25, No. 1, pp. 305–318.

Goldfain, B., Drews, P., You, C., Barulic, M., Velev, O., Tsiotras, P. and Rehg, J.M., 2019. "Autorally: An open platform for aggressive autonomous driving". *IEEE Control Systems Magazine*, Vol. 39, No. 1, pp. 26–55.

Jazar, R.N., 2008. *Vehicle dynamics*, Vol. 1. Springer.

Lemos, R.A., Sobral, G., Mirisola, L., Martins, R., Koyama, M. and de Paiva, E., 2017. "Estratégia de navegaçao autônoma entre fileiras de cultivares baseada em lasers". In *XIII Simpósio Brasileiro de Automaçao Inteligente*. Vol. 1.

Lutin, J.M., 2018. "Not if, but when: Autonomous driving and the future of transit". *Journal of Public Transportation*, Vol. 21, No. 1, pp. 92–103.

Nogueira, L.A.D.O., Koyama, M.F., Cordeiro, R.D.A., Ribeiro, A.M., Bueno, S.S. and DE Paiva, E.C., 2019. "A miniaturized four-wheel robotic vehicle for autonomous driving research in off-road scenarios". In *Congresso Brasileiro de Automática-CBA*. Vol. 1.

Polley, M. and Alleyne, A.G., 2004. "Dimensionless analysis of tire characteristics for vehicle dynamics studies". In *Proceedings of the 2004 American control conference*. IEEE, Vol. 4, pp. 3411–3416.

Rajamani, R., 2011. *Vehicle dynamics and control*. Springer Science & Business Media.

Ribeiro, A.M., Fioravanti, A.R., Moutinho, A. and de Paiva, E.C., 2022. "Nonlinear state-feedback design for vehicle lateral control using sum-of-squares programming". *Vehicle System Dynamics*, Vol. 60, No. 3, pp. 743–769.

Ribeiro, A., Koyama, M., Moutinho, A., de Paiva, E. and Fioravanti, A., 2021. "A comprehensive experimental validation of a scaled car-like vehicle: Lateral dynamics identification, stability analysis, and control application". *Control Engineering Practice*, Vol. 116, p. 104924. ISSN 0967-0661.

Schedlinski, C. and Link, M., 2001. "A survey of current inertia parameter identification methods". *Mechanical systems and signal processing*, Vol. 15, No. 1, pp. 189–211.

Sierra, C., Tseng, E., Jain, A. and Peng, H., 2006. "Cornering stiffness estimation based on vehicle lateral dynamics". *Vehicle System Dynamics*, Vol. 44, No. sup1, pp. 24–38.

Snider, J.M., 2009. "Automatic steering methods for autonomous automobile path tracking". *Robotics Institute, Pittsburgh, PA, Tech. Rep. CMU-RITR-09-08*.

Taylor, J., 1997. *Introduction to error analysis, the study of uncertainties in physical measurements*.

Uys, P., Els, P., Thoresson, M., Voigt, K. and Combrinck, W., 2006. "Experimental determination of moments of inertia for an off-road vehicle in a regular engineering laboratory". *International Journal of Mechanical Engineering Education*, Vol. 34, No. 4, pp. 291–314.

7. RESPONSIBILITY NOTICE

The authors are solely responsible for the printed material included in this paper.